Domain Shapes and Patterns: The Phenomenology of Modulated Phases

Michael Seul and David Andelman*

A wide variety of two- and three-dimensional physical-chemical systems display domain patterns in equilibrium. The phenomenology of these patterns, and of the shapes of their constituent domains, is reviewed here from a point of view that interprets these patterns as a manifestation of modulated phases. These phases are stabilized by competing interactions and are characterized by periodic spatial variations of the pertinent order parameter, the corresponding modulation period generally displaying a dependence on temperature and other external fields. This simple picture provides a unifying framework to account for striking and substantial similarities revealed in the prevalent "stripe" and "bubble" morphologies as well as in commonly observed, characteristic domain-shape instabilities. Several areas of particular current interest are discussed.

A surprisingly diverse set of physical and chemical systems exhibit macroscopic patterns and textures. In general, simple morphologies of some degree of regularity predominate: These include, notably, stripes and circular droplets ("bubbles") in two-dimensional (2D) systems, and sheets, tubes, and spherical droplets embedded in a homogeneous three-dimensional (3D) matrix. The predominance of a small set of morphological features leads to patterns of strikingly similar appearance, irrespective of the details of microscopic structure and interactions (*1*–*4*) (Fig. 1). Systems range in diversity from a type I superconducting film in its intermediate (equilibrium) state (Fig. 1A) to a (nonequilibrium) chemical mixture displaying complex steady-state reaction-diffusion (Turing) patterns (Fig. 1C). On the other hand, the characteristic scale, or period, of the patterns can vary from mesoscopic scales of hundreds of angstroms in ("ripple") phases of certain phospholipids (Fig. 1B) to as much as centimeters in convective roll patterns generated by a Rayleigh-Bénard instability (Fig. 1D).

Figures 2 and 3 depict examples of the simplest spatial configurations of textures observed in two and three dimensions (*5*–*11*). Linear arrays of stripes and hexagonal arrays of bubbles are ubiquitous in thin films of magnetic garnets (Fig. 2, A and B) (*12*, *13*) and in ferrofluids (Fig. 2, C and D). Stripe and bubble morphologies also arise in Langmuir films: These are insoluble monomolecular layers adsorbed at an air-water interface that are composed of amphiphilic molecules, such as phospholipids and fatty acids, whose polar groups endow them with a permanent (or induced) electric dipole moment (Fig. 3, A and B). Similarly, 3D assemblies of lipids as well as diblock copolymers adopt spatial distributions of constituents in the form of either sheets (lamellae) (Fig. 3C) or hexagonally arranged cylindrical tubes (Fig. 3D) (*14*).

The widespread appearance of macroscopic and mesoscopic equilibrium patterns displaying common structural features and exhibiting common modes of evolution suggests a possible universal mechanism to account for the formation of these textures. The approach we adopt here is to view them as a manifestation of modulated phases. Their periodic spatial organization is attributed to the presence of competing interactions favoring spatial inhomogeneities in an otherwise uniform ground state. In this picture, domains represent modulations in some order parameter (*15*), such as magnetization, as in epitaxial films of rare earth garnets, and polarization, as in ferroelectric films and Langmuir monolayers. The modulation period is set by the relative strengths of the competing interactions and can be tuned by varying parameters such as temperature and applied magnetic, electric, or other fields.

A wide variety of systems displaying patterns have all been analyzed within the framework of competing interactions (*16*–*34*) (Table 1). We comment in more detail on a number of these examples in the following sections. The related phenomena of structure formation in colloidal suspensions (*35*) and superlattice formation in adsor-

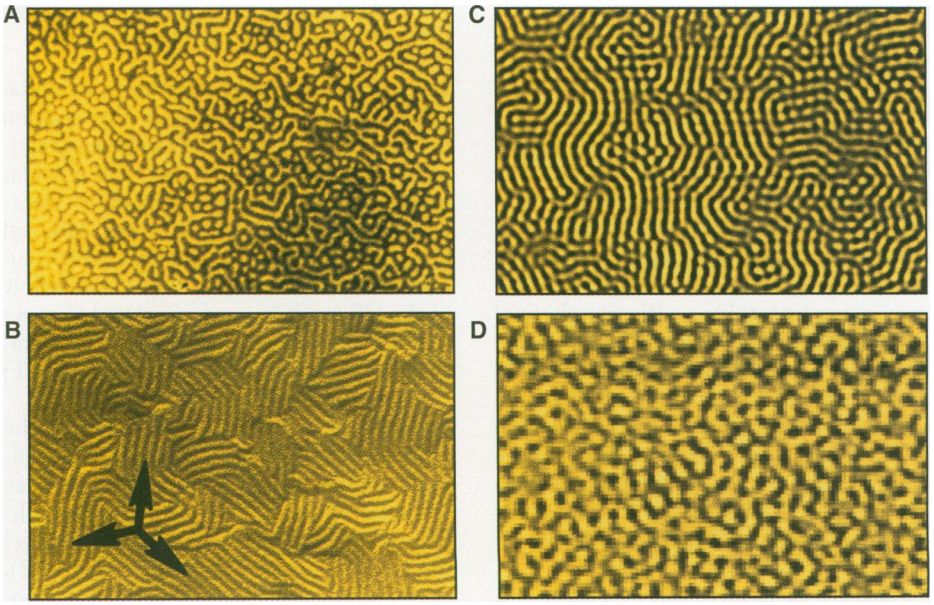

Fig. 1. Sampling of stripe domain patterns in physical and chemical systems. (**A**) Alternating superconducting and normal regions in a foil lead of a type I superconductor, in its intermediate state. The pattern was induced by a normal magnetic field and rendered visible by a powder decoration technique; period, ~7 μm. [Adapted from (*1*)] (**B**) $P_{\beta'}$ ("ripple") phase in a vesicle composed of the phospholipids dimyristoylphosphatidylcholine (DMPC) and dimyristoylphosphatidylethanolamine (DMPE) (95:5 molar ratio), rendered visible after rapid freezing by freeze-fracture electron microscopy; period, ~240 Å. [Adapted from (*2*)] (**C**) Stationary ("Turing") patterns in a chemical reaction-diffusion system, rendered visible by preferential absorption of light; period, ~0.25 mm. [Adapted from (*3*)] (**D**) Snapshot of fluctuations preceding the appearance of a convective roll pattern in CO_2 gas undergoing a Rayleigh-Bénard instability, rendered visible by a shadowgraph technique; period, ~1 cm. [Adapted from (*4*)]

M. Seul is at AT&T Bell Laboratories, Murray Hill, NJ 07974, USA. D. Andelman is at the School of Physics and Astronomy, Raymond and Beverly Sackler Faculty of Exact Sciences, Tel-Aviv University, Ramat-Aviv 69978, Israel.

*Also at Section de Physique et Chimie, Institut Curie 11, rue Pierre et Marie Curie, 75231 Paris Cedex 05, France.

bate films on crystalline substrates (36) have recently been reviewed elsewhere and will not be addressed here.

Competing Interactions and Modulated Structures

Interactions of long range. To illustrate the idea of modulated phases, we consider a 2D sheet on which two partially incompatible molecular species, say A and B, can diffuse laterally. For the purpose of this illustration, we assume that A and B molecules form an incompressible film that fully covers the sheet. The state of the system can then be characterized by selecting the relative composition (or mole fraction) ϕ to serve as an order parameter: $\phi = 1$ indicates a system of pure A composition, and $\phi = 0$ corresponds to pure B composition. The incompatibility of the molecular constituents will favor segregation into coexisting A-rich and B-rich phases, described by the respective values ϕ_A and ϕ_B of the order parameter and delineated by boundaries with line tension γ. This line tension expresses the energy cost incurred in forming boundaries between regions of differing composition and thus favors minimization of the total length of the boundary: As a result, A-rich and B-rich regions tend to grow.

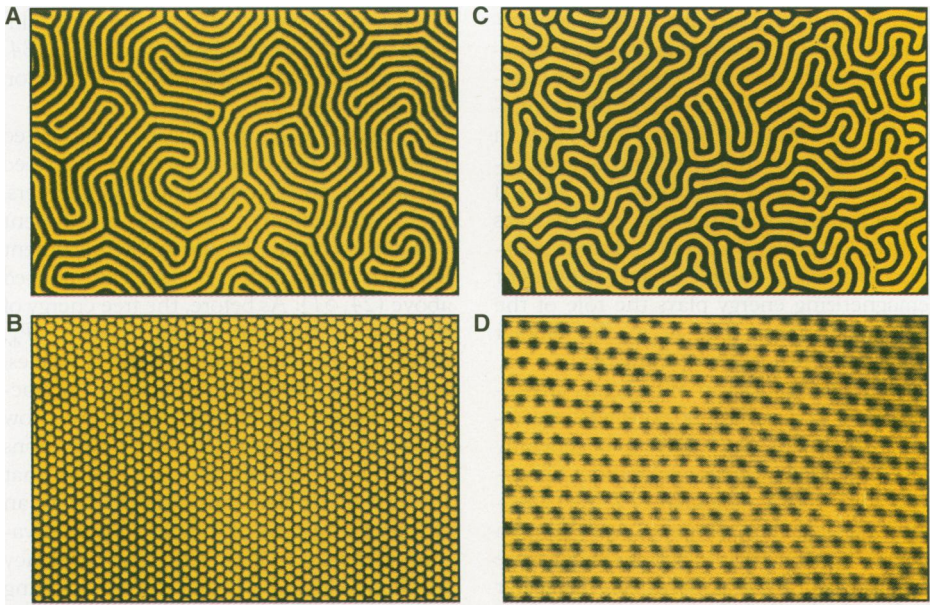

Fig. 2. Domains in magnetic solids and fluids. (**A**) Stripes and (**B**) bubble phase in ferromagnetic garnet film of 13 μm thickness grown on the ⟨111⟩ face of gadolinium gallium garnet (GGG), rendered visible by the Faraday effect; period, ~10 μm. [Adapted from (*5*)] (**C** and **D**) Ferrofluid confined between two glass plates in magnetic field normal to the fluid layer, exhibiting (C) labyrinthine [period, ~1 cm; adapted from (*6*)] and (D) bubble [period, ~4 μm; adapted from (*7*)] states.

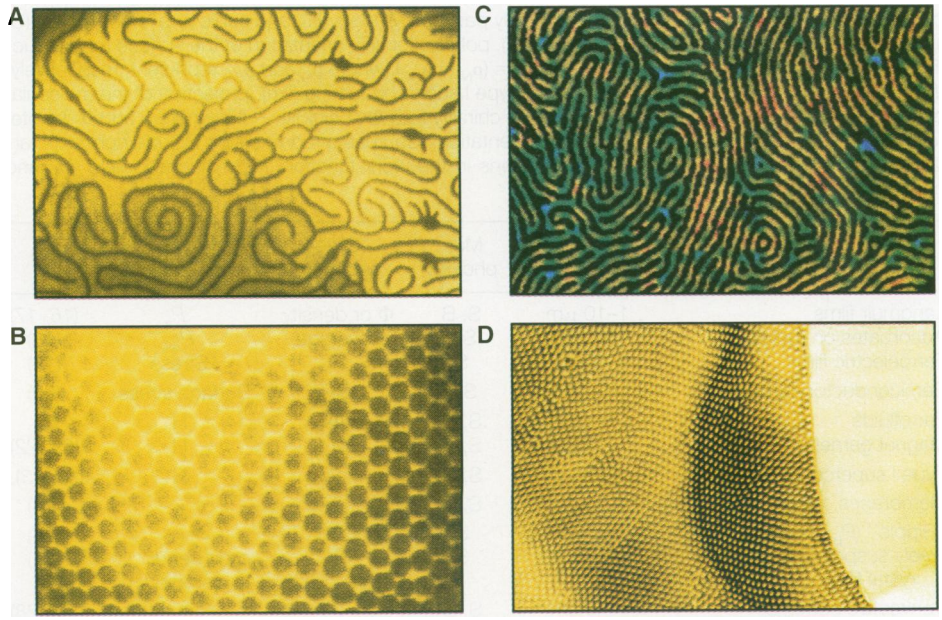

Fig. 3. Stripe and bubble domain phases in 2D and 3D organic systems. (**A** and **B**) Monomolecular organic (Langmuir) film, confined to an air-water interface, exhibiting (A) stripe [period, ~3.5 μm; adapted from (*8*)], and (B) bubble [period, ~20 μm; adapted from (*9*)] morphologies, rendered visible by fluorescence microscopy. (**C** and **D**) Solvent-cast film of block copolymers exhibiting (C) stripe [period, ~400 Å; adapted from (*10*)] and (D) bubble [period, ~160 Å; adapted from (*11*)] morphologies, the latter in the form of hexagonal arrays of cylindrical domains, rendered visible by heavy metal staining of thin sections imaged by transmission electron microscopy.

In the vicinity of the critical demixing point of A and B, the order parameter $\phi = \phi(\mathbf{r})$ and its spatial variations are small, and the free energy $\mathcal{F}_\phi$ of the mixture may be phenomenologically expressed as a (Ginzburg-Landau) expansion in powers of $\phi(\mathbf{r})$ and $\nabla\phi$

$$\mathcal{F}_\phi = \mathcal{F}_0[\phi] + \frac{1}{2}b\int d^2r\,|\nabla\phi|^2 = \mathcal{F}_0 + \gamma l \qquad (1)$$

where $\mathcal{F}_0$ captures (uniform) bulk contributions and assumes the form of a (Landau) expansion in powers of ϕ (*37*). The second term represents the energy cost associated with local variations in ϕ, notably those associated with domain walls. When these variations are small, the gradient-squared term with its "stiffness" coefficient b represents the lowest order approximation to the energy cost of creating the wall. In our 2D model, this wall energy is given simply as the product of line tension γ and domain wall length l.

This situation is substantially altered when the two species carry dipole moments μ_A and μ_B. For simplicity, we set one of the moments to zero: $\mu_B = 0$ and $\mu \equiv \mu_A$. If all molecular dipoles point along the direction normal to the sheet (Fig. 4A), they interact pairwise by means of a repulsive dipole-dipole electrostatic interaction. In the continuum limit, this dipole-dipole interaction may be represented in the form of an integral over the 2D monolayer

$$\mathcal{F}_d = -\frac{\mu^2}{2}\int\int d^2r\,d^2r'\,\phi(\mathbf{r})g(\mathbf{r},\mathbf{r}')\phi(\mathbf{r}') = -\frac{\mu^2}{2}\int d^2q\,\phi_{-q}G(q)\phi_q \qquad (2)$$

where the double spatial integral is taken over all possible dipole pairs (hence the prefactor of ½) and where $g(\mathbf{r}, \mathbf{r}') = |\mathbf{r} - \mathbf{r}'|^{-3}$ expresses the long-range nature of the dipole-dipole interaction. The sign of $\mathcal{F}_d$ is important: Its origin lies in the fact that Eq. 2 expresses the interaction energy of specific spatial configurations of a given (and hence fixed) number of dipoles, as compared to

that of a uniform spatial arrangement of the same set of dipoles (*38*). The second identity reflects a transformation of the double spatial integral into a single integral in Fourier space, which is always possible when $g(\mathbf{r}, \mathbf{r}') = g(|\mathbf{r} - \mathbf{r}'|)$; here, $G(q)$ and ϕ_q represent the (2D) Fourier transforms of $g(|\mathbf{r} - \mathbf{r}'|)$ and $\phi(\mathbf{r})$, respectively.

The combined free energy $\mathcal{F} = \mathcal{F}_\phi + \mathcal{F}_d$, obtained from Eqs. 1 and 2 with Fourier transform $F(q) = [-\mu^2 G(q) + bq^2]/2$, exhibits a minimum at a finite wave number $q^* \neq 0$ because $g(q)$ is positive and varies as $|q|$ for small q. This selection of an optimal q accounts for the emergence of a new length scale: Instead of macroscopic phase separation into A-rich and B-rich regions, we now expect the formation of a periodic pattern of alternating A-rich and B-rich domains. That is, the order parameter field $\phi(\mathbf{r})$ is spatially modulated as a result of the competition between the (nonlocal) dipolar interaction and the line tension (*39*).

The same considerations apply at low temperature for sharp domain walls. Whereas $\mathcal{F}_\phi$ may be reduced by an increase in domain size d (recalling that the two species are incompatible), $\mathcal{F}_d$ is reduced by the (continued) subdivision of domains. Consequently, the overall free energy, $\mathcal{F} = \mathcal{F}_\phi + \mathcal{F}_d$, favors (*16*, *17*) the formation of domains of a preferred size $d^* = d[\gamma/(\Delta P)^2]$, where $\Delta P = \mu(\phi_A - \phi_B)$ (*40*). The ratio $N_B \equiv (\Delta P)^2/\gamma$, generally referred to as the bond number, may be tuned by way of the temperature- or field-dependence of the pertinent interactions, with consequent adjustments in optimal domain size and modulation wavelength. As we will see below, N_B also governs the stability of shapes assumed by individual domains. The above model suggests a physical origin (*16*, *17*) of the patterns observed in Langmuir monolayers of amphiphiles carrying permanent molecular dipoles (Fig. 3, A and B). Patterns appear as temperature or lateral (surface) pressure is varied.

Although not phrased in this language, the idea of modulated phases with preselected equilibrium periodicity is expressed in the pioneering theories of spontaneous domain formation in magnetic materials (*21*, *41*) and in the intermediate state of type I superconductors (*23*). In the latter, the sample shape–dependent distribution of normal (N) and superconducting (S) regions is determined by the competition between the interfacial free energy γ_{SN} and a demagnetizing field (*42*). In a slab geometry, both droplet and stripe patterns are observed (*1*).

Nonlocal interactions associated with polarization, magnetization, and elastic strain have all been reported to lead to modulated phases. Polarization effects, related to variations in the work function between bare and adsorbate-decorated regions of a metal surface, have been shown to stabilize an equilibrium pattern of adsorbate domains on the surface (*18*). The interplay between polarization and elastic strain has been invoked to account for domain structures in epitaxial ferroelectric films (*19*) and in ferroelectric crystals (*43*). Furthermore, relaxation of surface strain has been proposed to account for the arrangement of certain reconstructed semiconductor surfaces in the form of domains of alternating orientations (*20*, *44*). A direct analogy may be drawn between polarization in the examples just discussed and magnetization in a thin layer of ferrofluid (*7*, *45*, *46*) and in a magnetic garnet film (*47*). In slabs of these (respectively liquid and solid) magnetic systems, a sample shape–dependent demagnetizing energy plays the role of the depolarizing term (Eq. 2) in the dipolar sheet model of Langmuir films (*47*).

Modulated phases in 3D systems are encountered in a variety of polymeric assemblies, where this phenomenon is generally referred to as microphase separation. Specifically in diblock copolymers (*29*, *30*), effective long-range interactions (equivalent in range to Coulombic interactions) reflect the connectivity of the copolymers' molecular blocks, which precludes compositional fluctuations on large length scales (*48*). Lamellar structures, hexagonal arrays of cylinders, and cubic arrays of spheres (along with more complex phases of cubic symmetry) have all been observed (*14*, *31*). These structures also form in mixtures of diblock copolymers and homopolymers (*32*) (see Fig 3, C and D), and lamellar and cellular patterns are expected for diblock copolymer films grafted to a surface (*49*). Recently, it has been recognized that even in systems as complex as blends of charged homopolymers, charged diblock copolymers (*33*), and aqueous solutions of weakly charged polyelectrolytes (*34*, *50*), spatial modulations in composition should be expected.

Coupled order parameters. Modulated phases may also arise in systems described by two (or more) coupled order parameters, each (individually) favoring a different equilibrium state. To illustrate the salient idea, we return to the 2D sheet introduced above (*24*, *51*). As before, the free energy of the system contains a contribution, $\mathcal{F}_\phi$, reflecting the demixing of A and B species. Instead of considering long-range interactions between molecular dipoles, we now allow for out-of-plane (bending) distortions of the sheet. Specifically, we assume that the two molecular constituents display an affinity for regions of different local curvature of the sheet (Fig. 4B). This tendency can be modeled by introducing a coupling term between the local composition $\phi(\mathbf{r})$ and the curvature of the sheet. Provided that distortions remain small, we may write

Table 1. Illustrative list emphasizing the wide variety and diversity of 2D and 3D systems in which modulated phases have been described. Morphologies are classified as stripes (S), islands (I), and bubbles (B) in 2D and as lamellae (L), hexagonally packed cylinders (H), and cubic arrays of spheres (C) in 3D. Order parameters include composition (Φ), polarization (P), orientation of the surface reconstruction (SR), normal magnetization (M_z), the ratio $\rho = (\rho_N = \rho_{SC})$ (where ρ_N and ρ_{SC} represent, respectively, the normal and superconducting fractions of a type I superconducting film), projection of the molecular director into the plane of the layer (*c*-dir), and the chirality field $\Psi = \sin[6(\varphi - \vartheta)]$ (where φ and ϑ denote, respectively, the tilt and bond field azimuthal orientation). Sources of competition include normal polarization (P_z), polarization associated with variations in the work function (P_{wf}), magnetic field (H), and curvature (κ).

System	Typical length scale	Morphology	Order parameter	Source of competition	Ref.
Langmuir films	1–10 μm	S, B	Φ or density	P_z	(*16*, *17*)
Adsorbates on metals	500 Å	S, I	coverage,	P_{wf}	(*18*)
Ferroelectric films	10 μm	S	P	Stress	(*19*)
Semiconductor surface	500 Å	S, I	SR	Surface stress	(*20*)
Ferrofluids	1 cm	S, B	Φ	H	(*6*)
Magnet garnets	10 μm	S, B	M_z	H	(*21*, *22*)
Type I superconductor films	10 μm	S, B	ρ	H	(*1*, *23*)
Membranes, vesicles	100 Å	S, B	Φ	κ	(*24*)
"Ripple" ($P_{\beta'}$) phase	100 Å	S	*c*-dir	κ	(*25*)
Freely suspended liquid crystal films	5 μm	S	Ψ	*c*-dir bend distortion	(*26*)
Convective patterns	1 cm	S, B			(*27*, *28*)
Turing patterns	1 cm	S, B			(*3*)
Diblock copolymers	500 Å	L, H, C	Φ	(Covalent) linkage	(*29–31*)
Co- and homopolymer mixture					(*32*)
Charged diblock copolymer Polyelectrolyte solution				Counterion entropy	(*33*) (*34*)

$$\mathcal{F}_c = \int d^2r \left[\frac{1}{2}\sigma |\nabla h(\mathbf{r})|^2 + \frac{1}{2}\kappa[\nabla^2 h(\mathbf{r})]^2 + \Lambda\phi(\mathbf{r})\nabla^2 h(\mathbf{r}) \right] \quad (3)$$

where $h(\mathbf{r})$ represents the height profile of the sheet (relative to a flat reference state), σ is its surface tension (not to be confused with the line tension introduced above for the flat monolayer), and κ is its bending modulus; Λ, the coefficient of the last term in the expression, measures the strength of the coupling of local curvature $\nabla^2 h$ and local composition ϕ, which we have included here to lowest (bilinear) order. This coupling term reflects the different affinities of the molecular constituents A and B of the model sketched in Fig. 4B for, respectively, convex ($\nabla^2 h > 0$) and concave ($\nabla^2 h < 0$) regions of the interface (*52*). This model describes a fluctuating fluid membrane. Minimization of the total free energy, $\mathcal{F} = \mathcal{F}_\phi + \mathcal{F}_c$ (Eqs. 1 and 3), with respect to the membrane shape $\{h(\mathbf{r})\}$ yields (*39*) an effective free energy that depends only on $\phi(\mathbf{r})$

$$\mathcal{F} - \mathcal{F}_0 = \int d^2r \left[\frac{1}{2}b' |\nabla\phi|^2 + \frac{\Lambda^2\kappa}{2\sigma^2}(\nabla^2\phi)^2 \right] = \int d^2q\, \phi_{-q}\tilde{G}(q)\phi_q \quad (4)$$

where $\mathcal{F}_0$ is defined in Eq. 1, $b' \equiv b - \Lambda^2/\sigma$, and in analogy to Eq. 2, $\tilde{G}(q) = (1/2)b'q^2 + (\Lambda^2\kappa/2\sigma^2)q^4$ is the 2D Fourier transform.

Note that the original stiffness coefficient b is replaced by a reduced coefficient b'. A negative b', obtained when $b < \Lambda^2/\sigma$, signals the onset of a curvature instability of the sheet. This instability generates a pattern of domains that differ in composition as well as in local curvature and thus assume convex or concave shapes. In complete analogy to the dipolar case (Eq. 2), the characteristic domain size corresponds to the existence of a minimum in the free energy at a nonzero wave number $q^* \approx 2\pi/d \neq 0$ (*39*). As before, d is set by the ratio of coefficients for the competing terms in the free energy: $d \simeq \sqrt{(\Lambda^2\kappa/\sigma^2)/|b'|}$.

The idea just sketched has been generalized to apply to two-component biological (bilayer) membranes and amphiphilic monolayers capable of shape deformations, as well as to deformations of cylindrical and spherical shapes of closed-form membranes (vesicles and liposomes) (*24*, *51*, *53*). Other generalizations involve the coupling between membrane curvature and spatial variations of the molecular tilt, as in a recent model (*25*) of the $P_{\beta'}$ (ripple) phase formed by certain phospholipids (Fig. 1B). A related model (*26*) considers the coupling between the variations in molecular tilt and a scalar chiral order parameter and may offer an explanation of recent observations of stable patterns in surface-ordered, freely suspended films of achiral liquid crystals (*54*). Similar ideas have been advanced to account for pattern formation in free-standing liquid crystal films composed of chiral molecules (*55*, *56*). Related models of coupled elastic interactions involving splay and twist distortions of the molecular tilt have been invoked to explain stripe patterns in nematic liquid crystal films in a magnetic field (*57*).

Stationary rolls (stripes) and hexagons (bubbles), displayed by nonequilibrium dissipative systems, notably those governed by competition between chemical reaction and diffusion (Fig. 1C) (*3*) and those exhibiting hydrodynamic instabilities (Fig. 1D) (*4*, *58*), may under certain conditions also be considered within the current framework (*59*).

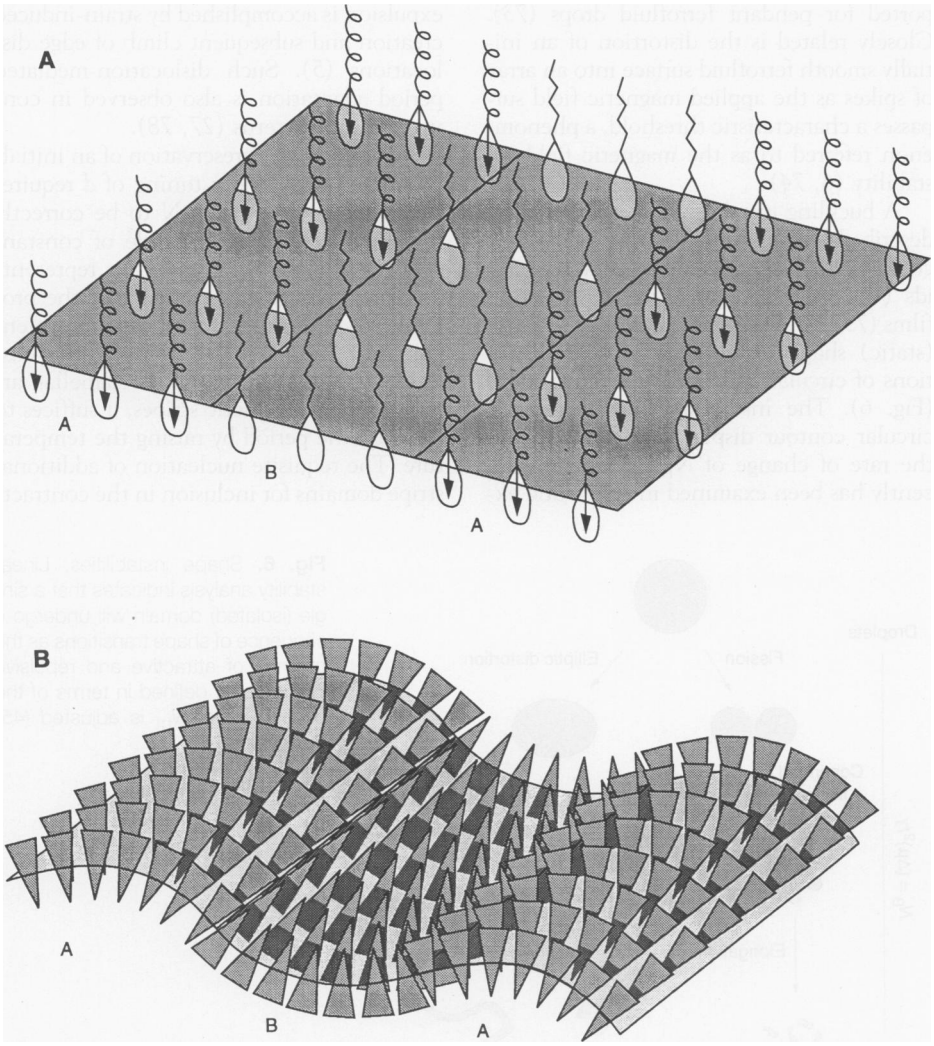

Fig. 4. Competing interactions on flat and curved interfaces. (**A**) Schematic representation of dipolar domains at the air-water interface. Dipole-dipole interactions stabilize a periodic arrangement of A-rich and B-rich domains; A and B are amphiphiles, assumed to carry dipole moments $\mu_A \gg \mu_B \simeq 0$. (**B**) Schematic representation of an undulating sheet (membrane), composed of two incompatible molecular species A and B. The packing of regular and inverted triangular shapes into A-rich and B-rich domains favors, respectively, convex and concave distortions of the membrane.

Generic Phase Diagram

Essentially equivalent mean-field theories for many of the systems discussed in the previous section have been based on a Ginzburg-Landau free energy functional of the form of Eq. 2 or Eq. 4 and on order parameter profiles in the form of simple sinusoidal modulations (*39*). The resulting phase diagram contains modulated stripe and bubble phases (*60*) separated by first-order phase transitions (Fig. 5). Similar phase diagrams have been derived for magnetic garnet films [modeled as a dipolar Ising ferromagnet] (*22*), Langmuir monolayers (*17*), adsorbates on metal surfaces (*18*), equilibrium shapes of two-component vesicles (*51*), and liquid crystal films of achiral molecules undergoing

chiral symmetry breaking (*26*). Moreover, a mean-field theory of diblock copolymers yields the 3D analog of this phase diagram, containing lamellar, cylindrical, and cubic phases (*14*, *29*), which are also expected for aqueous polyelectrolyte solutions (*34*, *50*).

Phase diagrams have also been calculated for the case of domains with sharp walls, encountered at low temperatures ($T \ll T_c$) (*61*). For magnetic garnet films, attempts have been made to connect the low-temperature and high-temperature regimes to predict, for example, the temperature dependence of the modulation period (*62*, *63*).

Order parameter fluctuations have been shown, in some cases, to eliminate the critical point from the phase diagram in favor of a (weakly) first-order phase transition, in a manner first suggested by Brazovskii (*64*). Pertinent analytical calculations as well as simulations have been performed for block copolymers (*65*), polyelectrolyte solutions (*50*), convective roll patterns (*58*), liquid crystal films with spontaneously broken chiral symmetry (*26*), and magnetic films (*66*). The essential deviation from mean-field behavior results from the emergence of an instability of the uniform (disordered) phase at finite wave number $q^* \neq 0$. Some experimental evidence for such fluctuations has been recently presented for block copolymers (*31*) and for Rayleigh-Bénard convection patterns (*4*, *27*).

Domain Shape Instabilities

In addition to controlling the period of condensed modulated phases, the balance of competing interactions also determines the stability of the shapes assumed by individual, isolated domains. Consider a single, 2D circular domain of dipoles, with dipoles oriented as in Fig. 4A and embedded in a nonpolar matrix. As long as line tension predominates, a circular domain shape will be preferred because this minimizes the length of domain boundary. As repulsive interactions between individual dipoles grow in relation to the line tension, that is, as the bond number N_B increases, instabilities ensue to produce elongated and branched shapes (Fig. 6) (*67*). The first such instability occurs at a critical (threshold) value of N_B when the circular domain becomes unstable to an elliptic distortion. A similar effect is observed when the domain size increases beyond a critical size with fixed N_B; this is a manifestation of the long range of the repulsive interaction.

Shape instabilities have been investigated theoretically and experimentally in a diverse set of systems including magnetic garnet films (*12*, *68*), ferrofluid layers (*6*, *45*, *69*), and Langmuir films (*70*–*72*); an elliptical shape distortion has also been reported for pendant ferrofluid drops (*73*). Closely related is the distortion of an initially smooth ferrofluid surface into an array of spikes as the applied magnetic field surpasses a characteristic threshold, a phenomenon referred to as the magnetic field instability (*6*, *74*).

A buckling instability of stripe domains, described long ago in films of type I superconductors (*1*), has been studied in ferrofluids (*45*) and more recently in Langmuir films (*75*). The most prevalent in a series of (static) shape instabilities involve distortions of circular and linear reference states (Fig. 6). The instabilities destabilizing a circular contour display a dependence on the rate of change of N_B, which only recently has been examined in systematic experiments on ferrofluid bubbles (*76*). As with Langmuir films, where qualitatively similar observations have been made (*72*), a more rapid rate of increase of N_B favors a higher symmetry (and shorter wavelength) of the dominant unstable mode.

Pattern Evolution and Disorder

We turn next to the evolution of patterns in response to adjustments of the modulation period d. In many cases, d varies inversely with N_B. The resulting strain must be accommodated by appropriate rearrangements of the existing domain pattern.

One of the simplest realizations of this phenomenon occurs in the ordered lamellar (stripe) domain phase of magnetic garnet films. Cooling in zero external field (Fig. 5) leads to an increase in d (*62*, *77*). For a film of fixed area, this implies that some lamellae must be eliminated from the pattern if the ordered state is to remain stable. This expulsion is accomplished by strain-induced creation and subsequent climb of edge dislocations (*5*). Such dislocation-mediated period adaptation is also observed in convective roll patterns (*27*, *78*).

In general, the preservation of an initially ordered state under tuning of d requires the number of domains N to be correctly matched, so that in a sample of constant area A_0, $Nd^2 \approx A_0$. In fact, this represents an exceptional circumstance, and the proliferation of disorder is a far more prevalent scenario. Thus, for the introduction of disorder in the aforementioned lamellar arrangement of magnetic stripes, it suffices to decrease the period by raising the temperature. The requisite nucleation of additional stripe domains for inclusion in the contract-

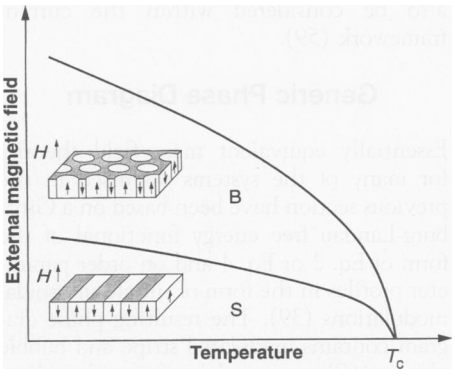

Fig. 5. Schematic mean-field phase diagram of modulated phases. Field-temperature (H-T) plane for a 2D system displaying stripe (S) and bubble (B) phases. The lines indicating first-order S-B and B-uniform phase transitions merge at a critical point T_c. Also indicated is the geometry of stripe and bubble arrays for magnetic garnet films (*22*); arrows indicate the magnetization direction.

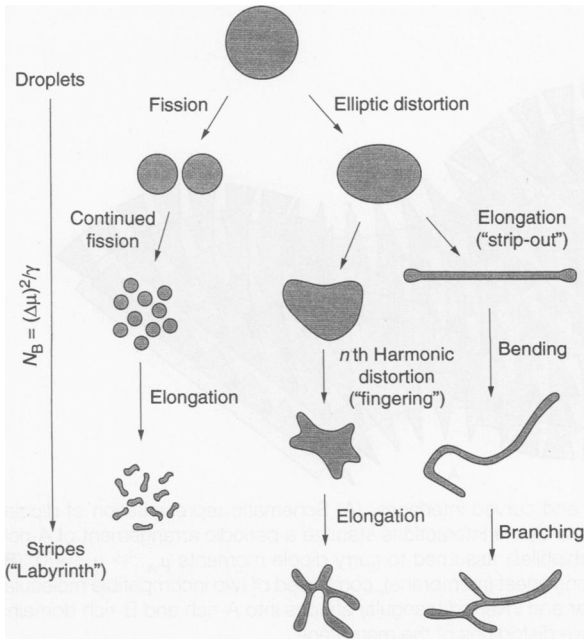

Fig. 6. Shape instabilities. Linear stability analysis indicates that a single (isolated) domain will undergo a sequence of shape transitions as the balance of attractive and repulsive interactions, defined in terms of the bond number N_B, is adjusted (*45*, *68*, *69*).

ing lamellar pattern is suppressed, and this constrains the number of stripes to remain fixed. To accommodate contraction under this constraint, the pattern undergoes a sequence of stripe bending and branching instabilities in response to the temperature-induced strain (*5*, *79*–*81*), reminiscent of an elastic response observed in smectic liquid crystal phases. Analogous zig-zag distortions are displayed by convective roll patterns (*28*, *82*) and various realizations of Turing patterns (*83*). A further increase in strain can lead to the formation of topological defects whose unbinding mediates the emergence of disordered, labyrinthine patterns (*5*). These reveal remarkable structural similarities to states of turbulence in dissipative systems (*3*, *58*, *83*).

An essential property of the patterns considered here is that they are composed not of rigid particles of fixed shape but rather of domains whose shape is susceptible to a variety of instabilities, as discussed above. A prominent instance of this coupling mediates the transformation between bubble and stripe patterns. This is predicated upon the elongation ("strip-out") of individual bubbles or, in the reverse direction, upon the rupture of stripes. The strip-out of individual bubble domains, triggered by an imposed period decrease under the constraint of maintaining a fixed number of domains, facilitates an identical evolution of a (multiply connected) disordered stripe domain pattern in magnetic garnet (*12*), as well as in Langmuir (*84*) films (Fig. 7), irrespective of details of molecular structure or composition.

The available experimental evidence supports the view that pattern evolution in response to period adjustment represents a constrained optimization problem; that is, pattern configurations are selected to realize the correct modulation period, dictated by the prevailing balance of competing interactions. Frequently, additional constraints of a rather general nature preclude the formation of the ordered state. In particular, the number of domains in a given pattern is generally difficult to change (see, for example, Fig. 7). The evolving disordered patterns represent alternative morphologies, selected by a constrained free-energy minimization. As in other "frustrated" systems, many configurations of essentially identical free energy may then exist.

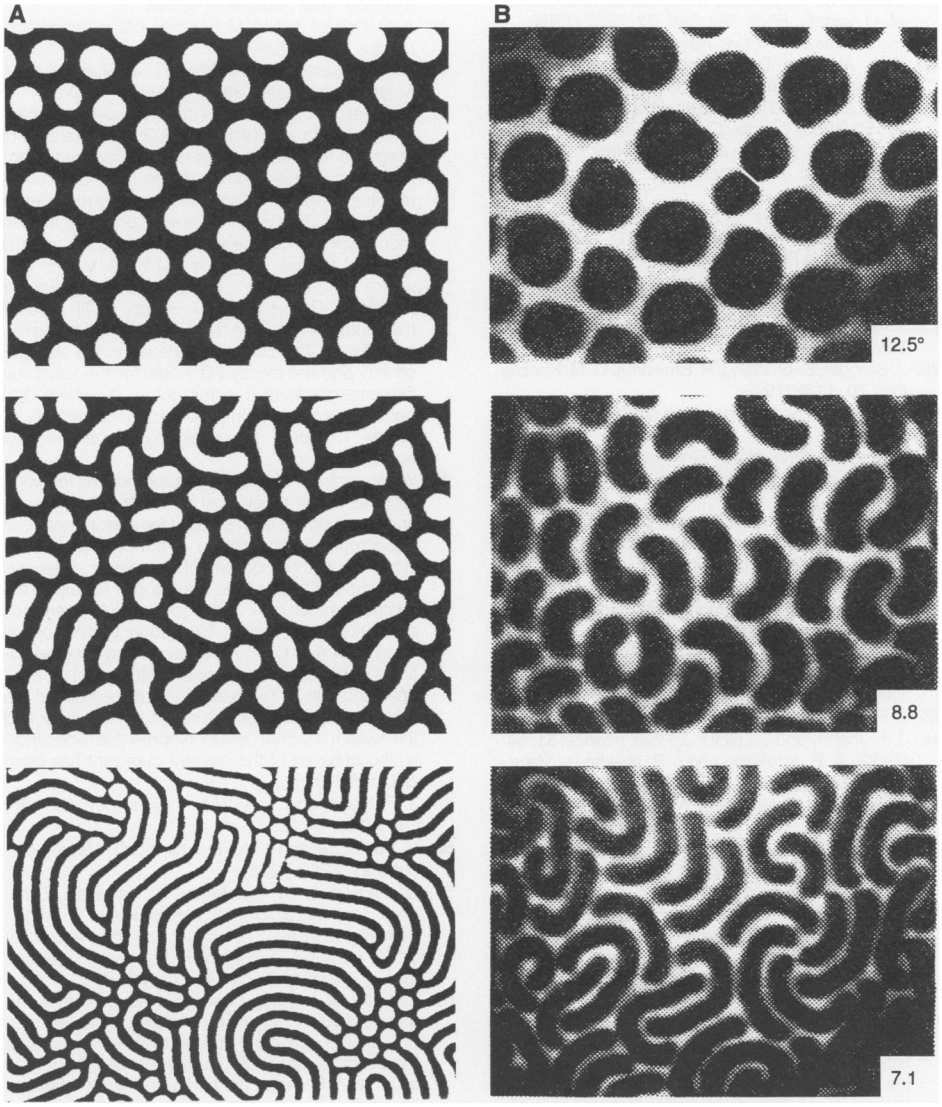

Fig. 7. Reversible "strip-out" instability in magnetic and organic thin films. Period reduction under the constraint of fixed overall composition and fixed number of domains leads to elongation of bubbles. (**A**) In magnetic garnet films, this is achieved (*96*) by raising the temperature [labeled in (B) in degrees Celsius] along the symmetry axis, $H = 0$ (period in bottom panel, ~10 μm) (see Fig. 5). (**B**) In Langmuir films, composed of the phospholipid dimyristoylphosphatidic acid (DMPA) and cholesterol (98:2 molar ratio, pH 11), this is achieved by lowering the temperature at constant average molecular density [period in bottom panel, ~20 μm, adapted from (*84*)].

Areas of Current Interest

Dynamic and kinetics of patterns and instabilities. Recent experimental efforts, for example, in ferrofluid films (*76*) and Langmuir films (*85*), have begun to address the dynamics of shape distortions in a quantitative way. As with structural features, striking similarities are beginning to emerge in the dynamics of domain shape instabilities in different systems. In contrast to the conventional case, spinodal decomposition in systems with competing interactions reflects the presence of an unstable mode (in equilibrium) at nonzero wave number (*86*), a feature previously alluded to in the context of the fluctuation spectrum in the uniform phase. These and other aspects of critical fluctuations, such as the determination of universality classes (*66*), are yet to be explored experimentally.

The nucleation of domains at the first-order phase transition from the uniform to the bubble phase, and the subsequent domain "ripening," is only now beginning to receive attention. Simulations on a variety of realizations of systems with competing interactions (*87*–*89*) reveal a crossover from an initial coarsening regime, dominated by the fastest growing unstable mode, to the periodically modulated equilibrium state. Coarsening in Langmuir films has been recently investigated experimentally (*90*). A related experimental investigation is the measurement of the rate of nucleation of individual bubble domains in a Langmuir film with a significant intralayer component of the molecular dipole (*91*).

Structural perturbations of modulated phases. The equilibrium structure of a given modulated phase may be subjected to a variety of perturbations arising from point impurities or line defects. A subtle effect of impurities on an ordered modulated phase is the destruction of true long-range positional order by random pinning (*92*). Disclina-

tion lines frequently occur in the director field describing the tilt configuration in films of tilted liquid crystals, and these have been shown to act as a structural perturbation on a coexisting modulated stripe phase, giving rise to a rather dramatic stripe defect pattern (*54*). The measurement of ("effective") elastic moduli of modulated phases might be feasible by probing the decay of imposed displacements of boundary layers (*93*). Interfaces between stripe, bubble, and uniform phases and the presence of external boundaries constitute another source of structural perturbation whose effects are currently under theoretical investigation.

Microscopic ordering and faceting of domains. Of particular interest to modulated phases in organic systems is the effect of molecular ordering of constituent molecules on the shape of domains. Given a proper understanding of the basic domain shape, deviations may actually serve to detect the presence or absence of molecular structure, as in the sixfold symmetric distortion ("faceting") of circular domains induced by a transition to a tilted phase of a Langmuir film (*94*). Molecular chirality is another microscopic property that has been demonstrated to affect stripe domains on macroscopic length scales: Elongating and branching stripes acquire a preferred handedness that is determined by the relative abundance of molecular enantiomers (*8*, *95*).

REFERENCES AND NOTES

1. R. P. Huebener, *Magnetic Flux Structures in Superconductors* (Springer-Verlag, Berlin, 1979); see also F. Haenssler and L. Rinderer, *Helv. Phys. Acta* **40**, 659 (1967); T. E. Faber, *Proc. R. Soc. London Ser. A* **248**, 460 (1958).
2. J. Zasadzinski and M. B. Schneider, *J. Phys. (France)* **48**, 2001 (1987).
3. Q. Ouyang and H. L. Swinney, *Nature* **352**, 610 (1991); *Chaos* **1**, 411 (1991).
4. E. Bodenschatz, J. R. de Bruyn, G. Ahlers, D. S. Cannell, *Phys. Rev. Lett.* **67**, 3078 (1991).
5. M. Seul, L. R. Monar, L. O'Gorman, *Philos. Mag. B* **66**, 471 (1992); _____ and R. Wolfe, *Science* **254**, 1616 (1991); M. Seul and R. Wolfe, *Phys. Rev. Lett.* **68**, 2460 (1992); *Phys. Rev. A* **46**, 7519 (1992); *ibid.*, p. 7534.
6. R. E. Rosensweig, *Ferrohydrodynamics* (Cambridge Univ. Press, Cambridge, 1985), chap. 7; *Sci. Am.* **247**, 136 (October 1982).
7. J. C. Bacri and D. Salin, *Endeavor New Ser.* **12**, 76 (1988).
8. R. M. Weis and H. M. McConnell, *J. Phys. Chem.* **89**, 4453 (1985); *Nature* **310**, 47 (1984).
9. M. Lösche and H. Möhwald, *Eur. Biophys. J.* **11**, 35 (1984), figure 4.
10. Figure 6 in E. N. Thomas and T. Witten, *Phys. Today* **21**, 27 (July 1990).
11. H. Hasegawa and T. Hashimoto, *Polymer* **33**, 475 (1992).
12. C. Kooy and U. Enz, *Philips Res. Rep.* **15**, 7 (1960); J. A. Cape and G. W. Lehman, *J. Appl. Phys.* **42**, 5732 (1971).
13. Bubble patterns in thin magnetic garnet films (Fig. 2B) have been extensively investigated in connection with potential technological applications of such materials, for example, in memory devices [T.H. O'Dell, *Rep. Prog. Phys.* **49**, 509 (1983); A. H. Eschenfelder, *Magnetic Bubble Technology* (Springer-Verlag, Berlin, 1980)].
14. More complex, three dimensionally modulated, so-called minimal surface (and related) phases [D. M. Anderson, H. T. David, L. E. Scriven, J. C. C. Nitsche, *Adv. Chem. Phys.* **77**, 337 (1990)] have also been described in surfactants [J. M. Seddon and R. H. Templer, *Philos. Trans. R. Soc. London Ser. A* **344**, 377 (1993)] and for diblock copolymers [E. N. Thomas, D. M. Anderson, C. S. Henke, D. Hoffman, *Nature* **334**, 589 (1988); M. W. Matsen and M. Schick, *Phys. Rev. Lett.* **72**, 2660 (1994)].
15. The order parameter, ψ, say, is a dimensionless measure of the degree of order in a system undergoing a phase transition from a disordered state (ψ = 0) to an ordered state (ψ = 1). For a detailed exposition, see L. D. Landau and E. M. Lifshitz, *Statistical Physics* (Pergamon, London, 1980).
16. D. J. Keller, H. M. McConnell, V. T. Moy, *J. Phys. Chem.* **90**, 2311 (1986); see also A. Fischer, M. Lösche, H. Möhwald, E. Sackmann, *J. Phys. Lett. (Paris)* **45**, L785 (1984); H. Möhwald, *Annu. Rev. Phys. Chem.* **41**, 441 (1990).
17. D. Andelman, F. Brochard, J.-F. Joanny, *J. Chem. Phys.* **86**, 3673 (1987); D. Andelman, F. Brochard, P. G. de Gennes, J.-F. Joanny, *C. R. Acad. Sci. (Paris)* **301**, 675 (1985).
18. D. A. Vanderbilt, *Surf. Sci.* **268**, L300 (1992); P. Zeppenfeld, M. Krzyzowski, C. Romainczyk, G. Comsa, M. G. Lagally, *Phys. Rev. Lett.* **72**, 2737 (1994).
19. B. S. Kwak *et al.*, *Phys. Rev. Lett.* **68**, 3733 (1992).
20. O. L. Alerhand, D. Vanderbilt, R. D. Meade, J. D. Joannopoulos, *ibid.* **61**, 1973 (1988).
21. L. D. Landau and E. M. Lifshitz, *Phys. Z. Sowjetunion* **8**, 153 (1935); *Landau Collected Papers* (no. 18), D. Ter Haar, Ed. (Gordon and Breach, New York, 1965).
22. T. Garel and S. Doniach, *Phys. Rev. B* **226**, 325 (1982).
23. L. D. Landau, *Phys. Z. Sowjetunion* **11**, 129 (1937); *Landau Collected Papers* (no. 30), D. Ter Haar, Ed. (Gordon and Breach, New York, 1965).
24. S. Leibler and D. Andelman, *J. Phys. (France)* **48**, 2013 (1987).
25. T. C. Lubensky and F. C. MacKintosh, *Phys. Rev. Lett.* **71**, 1565 (1993).
26. J. Selinger, Z.-G. Wang, R. Bruinsma, C. M. Knobler, *ibid.* **70**, 1139 (1993).
27. A. Weber, E. Bodenschatz, L. Kramer, *Adv. Mater.* **3**, 191 (1991).
28. W. Zimmermann, *Mater. Res. Soc. Bull.* **XVI**–special issue: *Complex Materials: Boojums at Work*, 46 (1991).
29. L. Leibler, *Macromolecules* **13**, 1602 (1980).
30. A. N. Semenov, *Sov. Phys. JETP* **61**, 733 (1985); T. Ohta and K. Kawasaki, *Macromolecules* **19**, 2621 (1986).
31. F. S. Bates and G. H. Fredrickson, *Annu. Rev. Phys. Chem.* **41**, 525 (1990).
32. T. Hashimoto, H. Tanaka, H. Hasegawa, *Macromolecules* **18**, 1864 (1985); H. Hasegawa, H. Tanaka, K. Yamasaki, T. Hashimoto, *ibid.* **20**, 1651 (1987).
33. J. F. Marko and Y. Rabin, *ibid.* **25**, 1503 (1992).
34. J.-F. Joanny and L. Leibler, *J. Phys. (France)* **51**, 545 (1990); A. R. Khokhlov and I. R. Nyrkhova, *Macromolecules* **25**, 1493 (1992).
35. J. Prost and F. Rondelez, *Nature* **350** (suppl.), 11 (1991).
36. W. Selke, *Phase Transitions and Critical Phenomena*, vol. 15, C. Domb and J. L. Lebowitz, Eds. (Academic Press, New York, 1992).
37. The expansion in powers of ϕ can be justified close to a critical point where the free energy of mixing contains only even powers in ϕ, $\mathcal{F}_0 = \frac{1}{2}t\phi^2 + \frac{1}{4}u\phi^4$; the parameter u is positive, and $t \approx T - T_c$ denotes the distance from the critical point T_c.
38. For a formal explanation, one may appeal to a Legendre transformation. This relies on a Lagrange multiplier to enforce the condition that the overall number of dipoles remains fixed when minimizing the free energy. This Lagrange multiplier P, coupled to the order parameter ϕ, generates a term of the form $\int P\phi(\mathbf{r})d^2r$, which must be added to the repulsive (and hence positive) dipole-dipole energy $(\mu^2/2)\int\int d^2r\, d^2r'\,\phi(\mathbf{r})g(\mathbf{r}, \mathbf{r}')\phi(\mathbf{r}')$. Optimizing with respect to $\phi(\mathbf{r})$, with fixed P, one recovers Eq. 2. This point is further explained in L. D. Landau and E. M. Lifshitz, *Electrodynamics of Continuous Media* (Pergamon, London, 1980).
39. Close to the critical point, the order parameter profile may be approximated by its most dominant q modes. In this single-mode approximation one thus considers only those modes corresponding to $q = |\mathbf{q}^*|$. The period of the domain pattern is then $2\pi/q^*$. In the context of phase separation phenomena, the regime in which this approximation applies is referred to as the weak-segregation limit: Domain boundaries are "diffuse" in the sense that their width is comparable to the domain period.
40. In the more general case where $\mu_A \neq \mu_B \neq 0$, ΔP is replaced by $(\mu_A - \mu_B)(\phi_A - \phi_B)$.
41. C. Kittel, *Phys. Rev.* **70**, 965 (1946).; *Rev. Mod. Phys.* **21**, 541 (1949).
42. The modulation period in a slab of thickness D obeys the approximate relation $d \approx D(\xi - \lambda)^{1/2}/\rho_N\rho_S$; ρ_N and $\rho_S = 1 - \rho_N$ respectively denote normal and superconducting volume fractions, and λ and ξ respectively represent the magnetic penetration depth and the superconducting coherence length. M. Tinkham, *Introduction to Superconductivity* (McGraw-Hill, Kogakusha, Tokyo, 1975), chaps. 1 and 3.
43. T. Mitsui and J. Furuichi, *Phys. Rev.* **90**, 193 (1953).
44. In contrast to the azimuthally symmetric nature of the electrostatic and magnetostatic interactions, elastic interactions are anisotropic and require a somewhat more complex treatment (*18*, *20*).
45. A. O. Cebers and M. M. Maiorov, *Magnetohydrodynamics* **16**, 21 (1980).
46. R. E. Rosensweig, M. Zahn, R. J. Shumovich, *J. Magn. Magn. Mater.* **39**, 127 (1983).
47. The slab geometry refers to a quasi–two-dimensional sample of finite thickness D. In such a layer of magnetic material, dipoles are induced by a magnetic field applied normal to the layer plane. The resulting demagnetizing energy may be modeled in the form of the Coulomb interaction between two monolayers of charge separated by a distance D (*22*, *45*); that is, $g(\mathbf{r}, \mathbf{r}') = 2(1/r - 1/\sqrt{r^2 + D^2})$, where $r \equiv |\mathbf{r} - \mathbf{r}'|$. The corresponding Fourier transform, $G(q) = (4\pi/q)[1 - \exp(-qD)]$, yields a minimum at finite $q^* \neq 0$ when balanced by $bq^2/2$, as in Eq. 2. The connection between the slab geometry and the strictly 2D model for the Langmuir film emerges from the limit $qD \ll 1$, where $G(q)$ behaves as $-|q|$. In the other limit of thick slabs, $qD \gg 1$, $G(q) \sim 1/q$, again favoring a preferred nonzero q^*.
48. We are grateful to T. Ohta for supplying the following argument: The topological connectivity between A and B monomers is reflected in the specific nature of the osmotic compressibility of the copolymer melt. While the number density of copolymer molecules (A-B dimers) in any finite volume can fluctuate, the relative number of A and B monomers, given their covalent linkage, cannot. Consequently, the volume fraction (of A or B monomer) evaluated over the entire system (that is, on a length scale $L \to \infty$) must be constant; that is, fluctuations in volume fraction are suppressed on large length scales, $q \sim 1/L \to 0$, and the system is osmotically incompressible. Specifically, the behavior of the relevant cumulant has been elucidated (*30*): $\langle\phi_q\phi_{-q}\rangle \sim q^2$.
49. J. F. Marko and T. A. Witten, *Phys. Rev. Lett.* **66**, 1541 (1991).
50. V. Yu. Borue and I. Ya. Erukhimovich, *Macromolecules* **21**, 3240 (1988).
51. D. Andelman, T. Kawakatsu, K. Kawasaki, *Europhys. Lett.* **19**, 57 (1992); T. Kawakatsu, D. Andelman, K. Kawasaki, T. Taniguchi, *J. Phys. II (France)* **3**, 971 (1993); T. Taniguchi, K. Kawasaki, D. Andelman, T. Kawakatsu, *ibid.* **4**, 1333 (1994).
52. The bilinear coupling between sheet curvature and composition in Eq. 3 is the lowest order term to differentiate between "up" and "down" regions of the interface, provided that there exists an intrinsic asymmetry between the two sides of the interface. This is the situation sketched in Fig. 4B, realized, for example, when the sheet represents a monomolecular layer of polar molecules with distinct "head" and "tail," or when the sheet separates two nonidentical fluid phases. In contrast, when there is "up-down" symmetry, as in cases involving a single-component molecular bilayer, the lowest coupling between curvature and composition is $\phi(\mathbf{r})[\nabla^2 h(\mathbf{r})]^2$.
53. M. Marder, H. L. Frisch, J. S. Langer, H. M. McCon-

nell, *Proc. Natl. Acad. Sci. U.S.A.* **81**, 6559 (1984).
54. J. Maclennan and M. Seul, *Phys. Rev. Lett.* **69**, 2082 (1992); *ibid.*, p. 3267; J. Maclennan, U. Sohling, N. A. Clark, M. Seul, *Phys. Rev. E* **49**, 3207 (1994).
55. S. A. Langer and J. P. Sethna, *Phys. Rev. A* **34**, 5035 (1986).
56. G. A. Hinshaw, R. G. Petschek, R. A. Pelcovits, *Phys. Rev. Lett.* **60**, 1864 (1988); G. A. Hinshaw and R. G. Petschek, *Phys. Rev. A* **39**, 5914 (1989).
57. G. Srajer, F. Lonberg, R. B. Meyer, *Phys. Rev. Lett.* **67**, 1102 (1991).
58. J. Swift and P. C. Hohenberg, *Phys. Rev. A* **15**, 319 (1977); P. C. Hohenberg and J. Swift, *ibid.* **46**, 4773 (1992); K. R. Elder, J. Viñals, M. Grant, *Phys. Rev. Lett.* **68**, 3024 (1992); *Phys. Rev. A* **46**, 7618 (1992).
59. In the vicinity of the first instability (of the uniform state), the dynamics of many dissipative systems are well described by variational evolution equations; that is, a functional $\mathcal{L}$ exists such that relaxational dynamics assume the form $\partial A/\partial t = -\delta\mathcal{L}/\delta A^*$. Here, A is a (generally complex) envelope function representing the spatial structure of the emerging pattern. The functional $\mathcal{L}$ may be expanded in terms of A and its spatial derivatives in a manner analogous to a Ginzburg-Landau expansion of the free energy in terms of an order parameter. The underlying periodicity of the pattern follows from a linear instability of the uniform state in a manner similar to the scenario of Eq. 4. M. C. Cross and P. C. Hohenberg, *Rev. Mod. Phys.* **65**, 851 (1993).
60. If a stripe phase is the manifestation of a unidirectional modulation, a bubble phase is obtained as a superposition of three stripe phases at proper relative orientation.
61. This case is characterized by domain boundaries whose widths are very much smaller than their size. In the context of phase separation phenomena, this regime is known as the strong-segregation limit.
62. W. A. Barker and G. A. Gehring, *J. Phys. C* **16**, 6415 (1983).
63. Although both stripe and hexagonal phases have been observed in different ferrofluid systems (Fig. 2), transitions between these two phases have not been observed. This is probably related to the high energy cost of forming the requisite transition states. For example, the stripe-to-hexagonal transition requires the fission of individual stripes, and this is observed only when long-range interactions are weak, as in certain Langmuir films [M. Seul and V. S. Chen, *Phys. Rev. Lett* **70**, 1658 (1993)] or, equivalently, when the temperature is high. In contrast, ferrofluids exhibit effectively zero-temperature behavior. In magnetic garnet films, the stripe-to-bubble transition is observed near the Curie temperature, T_c, whereas the transition is suppressed at lower temperatures.
64. S. A. Brazovskii, *Sov. Phys. JETP* **41**, 85 (1975) [*Zh. Eksp. Teor. Fiz.* **68**, 175 (1975)].
65. G. Fredrickson and E. Helfand, *J. Chem. Phys.* **87**, 697 (1987); M. Olvera de la Cruz, *Phys. Rev. Lett.* **67**, 85 (1991).
66. M. M. Hurley and S. J. Singer, *Phys. Rev. B* **46**, 5783 (1992).
67. Shape evolution by way of distortions is generally favored over fission (*63*).
68. A. A. Thiele, *Bell Syst. Tech. J.* **48**, 3287 (1969); *J. Appl. Phys.* **41**, 1139 (1970).
69. S. Langer, R. Goldstein, D. Jackson, *Phys. Rev. A* **46**, 4894 (1992).
70. H. M. McConnell, *Annu. Rev. Phys. Chem.* **42**, 171 (1991).
71. K. T. Vanderlick and H. Möhwald, *J. Phys. Chem.* **94**, 886 (1990); J. M. Deutsch and F. E. Low, *ibid.* **96**, 7097 (1992).
72. M. Seul and M. J. Sammon, *Phys. Rev. Lett.* **64**, 1903 (1990); M. Seul, *Physica A* **168**, 198 (1990).
73. J. C. Bacri and D. Salin, *J. Phys. Lett. (Paris)* **43**, L649 (1982); B. M. Berkovsky and V. I. Kalikmanov, *ibid.* **46**, L483 (1985).
74. As with the other instances of modulated phases discussed here, the array of spikes exhibits a periodicity that is determined by competing interactions. Specifically, these are the magnetic energy, which destabilizes the free surface, and the combined effects of gravity and surface tension, which favor a smooth (or flat) liquid surface. The instability, which is most dramatically observed in a planar geometry involving a pool of ferrofluid and a (vertical) magnetic field, was first analyzed by M. D. Cowley and R. E. Rosensweig [*J. Fluid Mech.* **30**, 671 (1967)].
75. K. J. Stine, C. M. Knobler, R. C. Desai, *Phys. Rev. Lett* **65**, 1004 (1990); F. Brochard-Wyart, *C. R. Acad. Sci. Paris Ser. II* **311**, 295 (1990).
76. A. J. Dickstein, S. Erramilli, R. E. Goldstein, D. P. Jackson, S. A. Langer, *Science* **261**, 1012 (1993); for a related theoretical analysis, see D. P. Jackson, R. E. Goldstein, A. O. Cebers, *Phys. Rev. E* **50**, 298 (1994).
77. This may be understood qualitatively by realizing that a decrease in temperature alters the balance of competing interactions in favor of the line tension, thereby favoring a reduction in interface length.
78. S. Rasenat, V. Steinberg, I. Rehberg, *Phys. Rev. A* **42**, 5998 (1990); for a recent review, see, for example, I. Rehberg *et al.*, *Festkoerperprobleme* **29**, 35 (1989).
79. P. Molho, J. L. Porteseil, Y. Souche, J. Gouzerh, J. C. S. Levy, *J. Appl. Phys.* **61**, 4188 (1987).
80. D. Sornette, *J. Phys. (France)* **48**, 151 (1987); *ibid.*, p. 1413.
81. S. J. Singer, *Phys. Rev. E* **48**, 2796 (1993).
82. M. Manneville, *Dissipative Structures and Weak Turbulence* (Academic Press, Boston, MA, 1990), chaps. 4 and 9.
83. V. Dufiet and J. Boissonade, *Physica A* **188**, 158 (1992).
84. W. M. Heckl and H. Möhwald, *Ber. Bunsenges. Phys. Chem.* **90**, 1159 (1986).
85. D. J. Benvegnu and H. M. McConnell, *J. Phys. Chem.* **96**, 6820 (1992); M. Seul, *ibid.* **97**, 2941 (1993); R. E. Goldstein and D. P. Jackson, *ibid.* **98**, 9626 (1994).
86. F. Brochard, J.-F. Joanny, D. Andelman, in *Physics of Amphiphilic Layers*, J. Meunier, D. Langevin, N. Boccara, Eds. (Springer-Verlag, Berlin, 1987).
87. C. Roland and R. C. Desai, *Phys. Rev. B* **28**, 6658 (1991); C. M. Sagui and R. C. Desai, *Phys. Rev. Lett.* **71**, 3995 (1993); *Phys. Rev. E* **49**, 2225 (1994).
88. L. Q. Chen and A. G. Khatchaturyan, *Phys. Rev. Lett.* **70**, 1477 (1993).
89. M. Bahiana and Y. Oono, *Phys. Rev. A* **41**, 6763 (1990).
90. M. Seul, N. Y. Morgan, C. Sire, *Phys. Rev. Lett.* **73**, 2284 (1994).
91. P. Muller and F. Gallet, *ibid.* **67**, 1106 (1991); *J. Phys. Chem.* **95**, 3257 (1991).
92. R. Seshadri and R. M. Westervelt, *Phys. Rev. Lett.* **66**, 2775 (1991); *Phys. Rev. B* **46**, 5142 (1992); *ibid.*, p. 5150.
93. R. Seshadri and R. M. Westervelt, *Phys. Rev. Lett.* **70**, 234 (1993); *Phys. Rev. B* **47**, 8620 (1993).
94. C. M. Knobler and R. C. Desai, *Annu. Rev. Phys. Chem.* **43**, 207 (1992).
95. H. E. Gaub, V. T. Moy, H. M. McConnell, *J. Phys. Chem.* **90**, 1721 (1986).
96. M. Seul, unpublished results.
97. We have greatly benefited from the advice and support of our collaborators and numerous colleagues. We are especially grateful to those who have made available material for references and photographs reproduced in this article and to D. Chatenay, T. Garel, P. Hohenberg, and T. Ohta for a critical reading of and comments on this manuscript. S. Cullerton's expertise in electronic photographic production techniques was invaluable. D.A. would like to acknowledge partial support from the German-Israel Foundation under grant I-0197 at Tel-Aviv University and from the Henri de Rothschild Foundation at Institut Curie.

HIV Population Dynamics in Vivo: Implications for Genetic Variation, Pathogenesis, and Therapy

John M. Coffin

Several recent reports indicate that the long, clinically latent phase that characterizes human immunodeficiency virus (HIV) infection of humans is not a period of viral inactivity, but an active process in which cells are being infected and dying at a high rate and in large numbers. These results lead to a simple steady-state model in which infection, cell death, and cell replacement are in balance, and imply that the unique feature of HIV is the extraordinarily large number of replication cycles that occur during infection of a single individual. This turnover drives both the pathogenic process and (even more than mutation rate) the development of genetic variation. This variation includes the inevitable and, in principle, predictable accumulation of mutations such as those conferring resistance to antiviral drugs whose presence before therapy must be considered in the design of therapeutic strategies.

Despite an extensive international research effort, HIV infection remains incurable and only modestly treatable. The infection of humans with this virus is characterized by three phases (*1–4*). Within several weeks after infection, there is an early phase with acute symptoms, extensive viremia, and large numbers of infected CD4-positive T cells in blood. Roughly coincident with the onset of the antiviral immune response (which includes antibodies and cytotoxic T cells), the amount of circulating virus declines by a factor of 100 or more (*5, 6*), leading to a clinically latent phase of variable duration with low but constant amounts of virus and infected cells in circulation and, usually, very gradually declining numbers of $CD4^+$ T cells. After about 10 years of clinical latency, the number of $CD4^+$ T cells declines to very low values and the symptoms of acquired immunode-

The author is in the Department of Molecular Biology and Microbiology, Tufts University School of Medicine, 136 Harrison Avenue, Boston, MA 02111, USA.